PATIENT-SPECIFIC MODELING AND VISUALIZATION OF BLOOD FLOW THROUGH THE HEART

Scott Kulp[⋆] *Dimitris Metaxas*[⋆] *Zhen Qian* [†] *Szilard Voros*[†] *Leon Axel*[‡] *Viorel Mihalef*[⋆]

[⋆] Department of Computer Science, Rutgers University, New Brunswick, NJ
[†] Piedmont Heart Institute, Piedmont Healthcare, Atlanta, GA
[‡] Department of Radiology, NYU School of Medicine, New York, NY

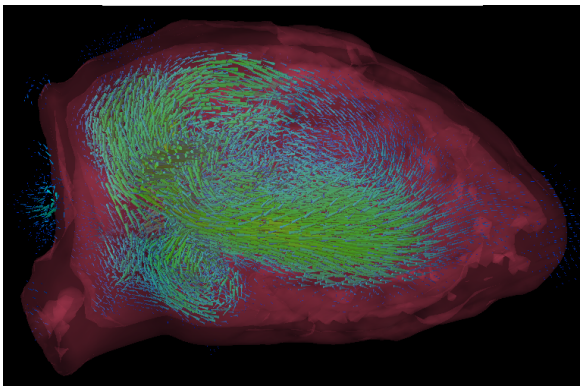

Fig. 1. Velocity field visualization of full heart before systole

ABSTRACT

Many cardiovascular diseases, such as ischemia and arrhythmia, will cause abnormal motion of the myocardium, leading to a change of the blood flow pattern in the heart and an increased risk of the formation of thrombus. In this paper, we propose a new method to use high-resolution 4D CT data to model the complex moving boundaries of the heart walls, accurately simulate blood flow using the Navier-Stokes equations, and visualize the flow in order to view interactions between the heart walls and the fluid. We then visually and quantitatively compare the flow in a normal heart to that of a heart suffering from hypokinesis, and see how the diseased heart is at greater risk of blood clotting. In a clinical setting, these types of visualizations could prove to be invaluable, allowing doctors to more easily diagnose and prescribe treatments for certain conditions.

Index Terms— Blood flow, CT, cardiac, hypokinesis

1. INTRODUCTION AND RELATED WORK

Currently, valvular blood flow can be monitored using imaging techniques such as Doppler ultrasound and MRI. However, the spatial resolutions of such techniques are low, and it is not possible to observe the detailed interaction of the blood flow and the endo-cardial surface of the heart, so the formation of cardiac thrombus remains difficult to predict. If a physician were able to visualize or quantitatively measure the detailed alteration of the blood flow by altered contraction, he might be able to make a better diagnosis or treatment plan. Therefore, in this paper, we seek to find ways to perform flow modeling and visualizations, given a 3D model of a heart.

With the rapid development of high-resolution cardiac CT, patient-specific blood flow simulation is quickly becoming one of the central goals in the study of cardiac blood flow. Recently [1] have published a framework for simulating atrioventricular blood flow, and showed simulation results using a complete model of the left side of the heart, including the atrial venae and an aortic stub, together with modeled valve kinematics. Later, [2] used smoothed 4D CT data to simulate left ventricular blood flow, and compared the flow around through the aortic valve in a healthy heart and two diseased hearts. Our paper is influenced by these works, and we improve the heart model by using higher-quality CT scans of normal subjects and live patients with cardiovascular disease that allow us to capture the complex details of the heart walls and trabeculae. In contrast, the geometry used in [1] was obtained from scans based on data from the Visible Human Project [3], while the kinematics was transfered to the model from MRI data, and the models derived from CT data in [2] were highly smoothed and were not useful for understanding the true interactions between the blood flow and the walls.

Earlier work in blood flow simulation used less refined models. For example, [4] was the first to extract boundaries from MRI data to perform patient-specific blood flow simulations. Later, [5] and [6] used simple models of the left side of the heart, with smooth ventricular walls, and imposed boundary conditions in the valve regions. Our approach (similarly to the one in [1]) uses predefined motion for the valves, whose asynchronous opening and closing provides a simple geometric mechanism for taking care of those boundary conditions. This approach relies on the reasonable assumption that the left ventricle drives essentially all of the dynamics of the blood flow in the left side of the heart.

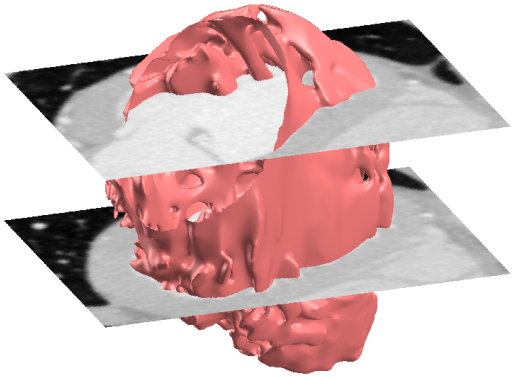

Fig. 2. View of a detailed mesh extracted from CT data using isosurfacing. Note the complex trabeculae inside the heart.

Our paper is organized as follows: In Section 2, we describe the high-resolution CT scanner that we use to capture the 4D data and the methods we use to extract the heart mesh. In Section 3, we discuss the fluid simulation system we use to solve the Navier-Stokes equations and very accurately model the flow through the heart. In Section 4, we demonstrate several ways in which we visualize the blood flow and view the interactions between the fluid and the highly complex surface of the heart. In Section 5, we describe our results after applying the visualizations techniques on a blood flow simulation through a healthy heart, and compare the simulated flows of a normal heart and one suffering from hypokinesis in the apical region. Finally, in Section 6, we present our conclusions and discuss our future work.

2. DATA AQUISITION

The CT images were acquired on a 320-MSCT scanner (Toshiba Aquilion ONE, Toshiba Medical Systems Corporation). This advanced diagnostic imaging system is a dynamic volume CT scanner that captures a whole-heart scan in a single rotation, and achieves an isotropic 0.5mm volumetric resolution with less motion artifact than the conventional 64-MSCT scanners. A conventional contrast-enhanced CT angiography protocol was adapted to acquire the CT data in this work. After the intravenous injection of the contrast agent, the 3D+time CT data were acquired in a single heart beat cycle when the contrast agent was circulated to the left ventricle and aorta, so that we were able to achieve an optimal intensity difference level between the blood pool and the left ventricular myocardium. After acquisition, 3D images were reconstructed at 10 time phases in between the R-to-R waves using ECG gating. The acquired isotropic data had an in-plane dimension of 512 by 512 pixels, with an effective atrio-ventricular region measuring about 300^3 pixels.

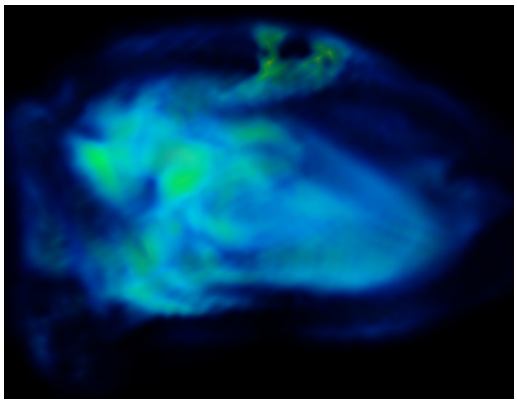

Fig. 3. Vorticity field visualization of full heart. Green regions correspond to higher magnitudes of vorticity and thus greater rates of rotation. Compare to figure 1, taken at the same time step.

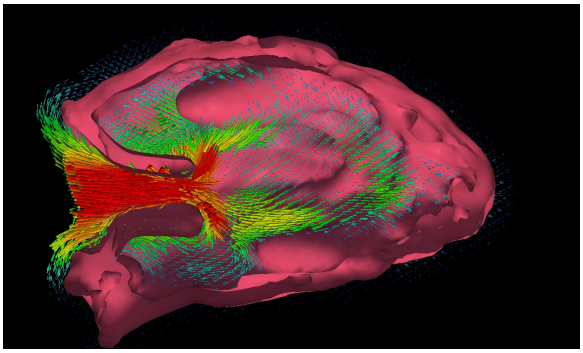

Fig. 4. Cross-section of heart during late diastole

The left ventricle region was extracted from the dataset using an initial median filtering, followed by isosurfacing and mesh cleanup and smoothing. The highly complex surface was extracted at mid diastole, and its motion was transfered from the smooth mesh motion obtained from the same CT data. An example mesh can be seen in figure 2, where we can clearly see the detailed trabeculae interior to the heart.

3. SIMULATION SYSTEM

The motion of an incompressible fluid is governed by the laws of conservation of momentum and mass. These two laws are modeled by the Navier-Stokes equations:

$$\rho(\tfrac{\partial u}{\partial t} + u \cdot \nabla u) = -\nabla P + \mu \nabla^2 u$$
$$\nabla \cdot u = 0$$

The first equation enforces conservation of momentum. Here, ρ is the fluid density, u is the 3D velocity vector field, P is the scalar pressure field, and μ is the coefficient of viscosity. The second equation states that the divergence of ve-

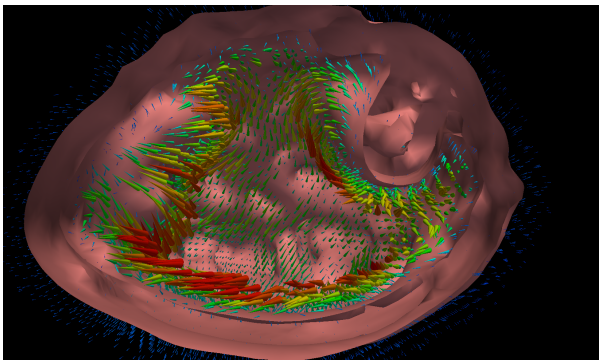

Fig. 5. Cross-section view of apical region during systole. Only fluid velocities directly against the heart walls are displayed, in order to more clearly see the complex interactions.

locity is zero everywhere, and thus there are no sources or sinks anywhere in the flow, conserving mass.

Foster and Metaxas [7] were the first to develop a very fast method of solving the Navier-Stokes equations for graphics applications. They did so by applying a staggered grid across the domain and explicitly solving for the three components of velocity at the cell faces. They then used successive over-relaxation to solve for pressure and correct the velocities to maintain incompressibility.

Our fluid-solid interaction system uses a "boundary immersed in a Cartesian grid formulation", which allows an easy treatment of complex geometries embedded in the computational domain, especially advantageous when dealing with moving boundaries. Recent work that employs such a formulaton is [8] and [9], which applies the formulation of [10] to both graphics and medical simulations. Very recently [11] implemented the approach of [12] to obtain a system that can efficiently deal with rather complex geometric data like a system of blood vessels.

In our solver, we use the methods similar to those described in [1]. The 3D mesh we generate from CT data is represented by a marker level set, introduced and validated in [13]. Here, markers are placed on the boundary, and are used to correct the level set at every time step. The marker level set approach is similar to the particle level set method ([14]), but since markers are only placed only on the surface, MLS has been proven to be more efficient and significantly more accurate for complex boundaries. Additionally, our specific solver achieves efficiency by implementing a parallel and adaptive mesh refinement approach, similar to the one proposed in [10].

The heart models used here are embedded in a computational mesh of 100^3 cells on which the full Navier-Stokes equations with a viscous component are solved using finite difference method. The blood is modeled as a Newtonian fluid, with viscosity set at 4mPa$\cdot$ s and density set at 1060kg/m^3, which are physiologically accepted values for a normal patient. The heart geometric model is fed to the solver as a discrete set of meshes with point correspondences, which allow easy temporal interpolation and also obtaining the velocity of the heart mesh at every point in time. The heart mesh and its velocity are rasterized onto the Eulerian grid as a marker level set, respectively as an Eulerian velocity (subsequently extrapolated onto a MAC grid). The marker level set and the velocity are used to impose the appropriate boundary conditions to the fluid solver. Treatment of and issues related to the simulation of the isovolumic stages are discussed in [1].

3.1. Validation

We qualitatively validated the results of our simulation by the inspection and visual verification of several doctors. In addition, as we have mentioned, our simulation methods have been proven in [13] to be extremely accurate, and numerical phantoms have been used to validate the software. It is possible to noninvasively obtain velocity data from MRI data, but it is prone to error and can only be retrieved in one direction. In the future, we plan to use phantoms to perform validation of these results.

4. VISUALIZATION METHODS

As mentioned previously, we adapted the framework described in [1] to perform the fluid simulation. With the fluid velocity fields and level sets generated for each time step, we use Paraview to visualize the simulations. On a machine with a Core 2 Quad processor and 8GB of RAM, each of the visualizations typically take 15-30 minutes to render 83 frames. We analyzed five healthy hearts and we describe below our visualization methods and our results. The fluid velocities of the five normal hearts at each time step were within $\pm 10\%$ of one another. We also visualized flows in a simulated diseased heart suffering from a large perfusion defect area created by reducing motion in the anterior apical area, as would be expected from ischemia or infarction in the distribution of the left anterior descending coronary artery.

4.1. Full Heart

We first performed a visualization of the velocity field of the entire heart, as seen in figure 1. The velocity of the blood at a given point is represented by a cone pointed in the direction of the flow. A cone's size increases linearly as the magnitude of the velocity increases. Additionally, we adjust the color of a cone by first setting its hue to 160 (blue), and then linearly lowering this value to a minimum of 0 (red) as velocity increases.

We then used finite differencing to compute the flow's vorticity at every point in the field. We use the magnitudes to create a volumetric visualization of vorticity, where brighter

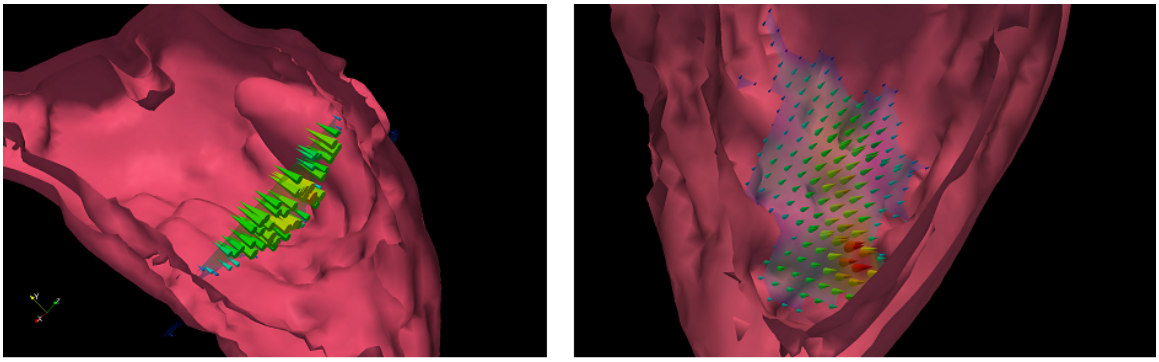

(a) (b)

Fig. 6. Left: visualization of flux through the apex of the heart during systole; Right: velocity field directly against trabeculae during systole

areas are associated with higher vorticites and greater rates of rotation and circulation.

4.2. Cross-Section

Next, we examined cross-sections of the heart, and visualized the velocities here. This way, we have a clearer picture of how each of the structures and trabeculae affect the flow of blood. We visualized the velocity field in the same way as above, representing the velocity at each point with a colored cone. Screenshots of the visualization can be seen in figures 4 and 5.

4.3. Flux

In the previous two sets of visualizations, we have seen how the complex structure of the walls of the heart affects the flow of blood. We now introduce two additional methods we use to visualize the flux across a certain region. To do this, we simply inserted a plane at the desired location and orientation, interpolated to sample the velocities across the plane, and projected the velocities onto the plane's normal vector. Two examples can be seen in figure 6.

5. RESULTS AND DISCUSSION

5.1. Visualizations of Healthy Heart

5.1.1. Full Heart

The visualizations of the velocity field and the vorticity field for the entire heart can be seen in figures 1 and 3, respectively. The images generated from visualizing the vorticity are visually stunning. We see in figure 3, the areas with the largest vorticities are close to the base, near the papillary muscles and the valves, which suggests that the fluid is spinning more rapidly here. Note that in figure 1, which is the velocity field taken at the same time step as that in figure 1, we see a number of large spirals in the same location.

5.1.2. Cross-Sections

As displayed in figures 4 and 5, the cross-section visualization allows us to see the interactions between the blood flow and the complex heart walls, which, to the best of our knowledge, has never been possible before. In our full animation, we can see how blood moves through and around the trabeculae, the papillary muscles, and the valves during the entire cardiac cycle. This is far more accurate than earlier attempts of cardiac blood flow simulations with smooth walls, and we can use this to find problems with diseased hearts, such as stagnant fluid in the trabeculae that increases the risk of thrombosis. In a later section, we use this way of visualizing flow to compare the the blood flow of a healthy heart to that of a diseased heart, demonstrating its potential clinical use.

5.1.3. Flux

To test the flux visualization method, we place planes at two different locations. First, we place a flux plane near the apex of the heart and visualize the flow across it. In figure 6 (a), we see the flux across this region during ventricular systole. We then insert a flux plane directly against the trabeculae of the heart walls. From figure 6 (right), we can clearly see how, during ventricular systole, the trabeculae contract, expelling the blood. In the future, we plan to run additional simulations on diseased hearts whose trabeculae do not contract. We will be using these methods of visualization in order to determine if blood remains trapped, leaving the patient at greater risk of a blood clot.

5.2. Comparison Between Normal and Diseased Heart

We now compare the flow fields of a healthy heart to that of a diseased heart, whose apex does not contract properly during ventricular systole. In figure 7, we show both hearts at three different stages of the heart cycle. The top row displays a normal heart, and the bottom row displays the diseased heart.

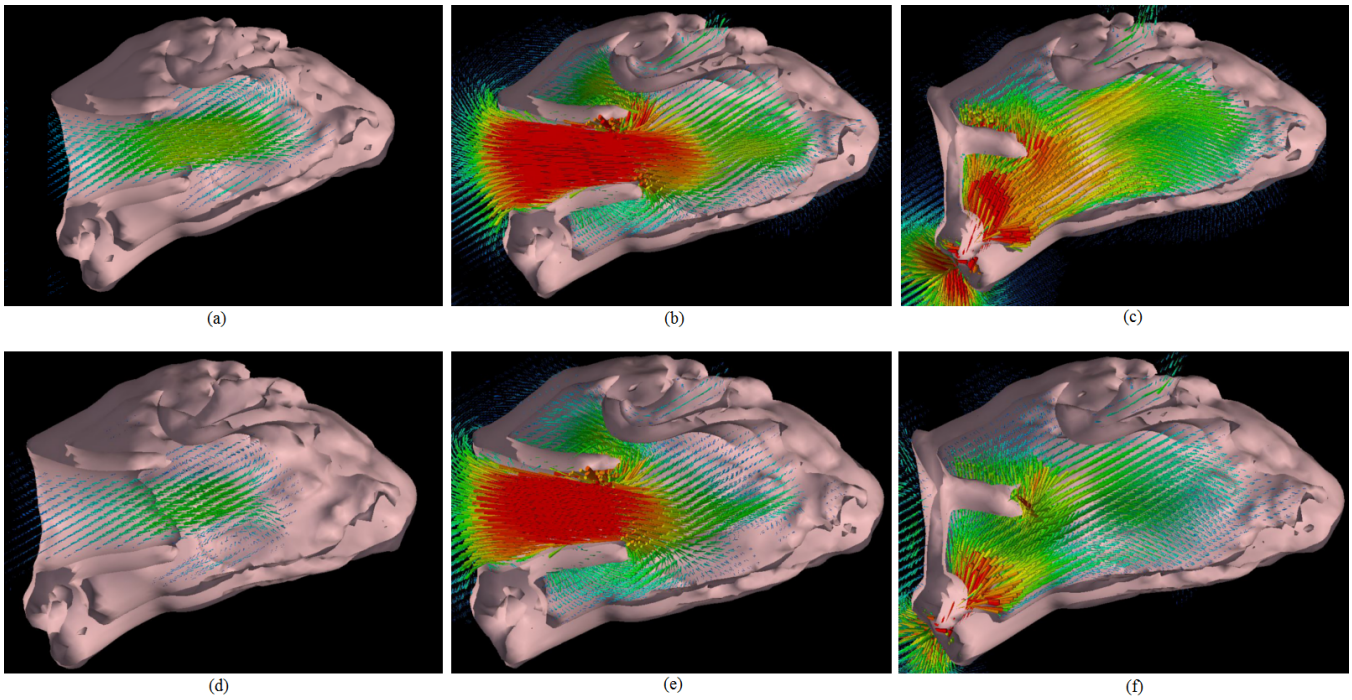

Fig. 7. Comparison of blood flow between a normal heart (top) and a diseased heart with hypokinesis in the apical region (bottom). First column: Mid diastole; Second column: Late diastole; Third column: Systole. Note how that in all three stages, the blood in the apical region remains relatively stagnant in the diseased heart, increasing the risk of clotting. We also note that the apex of the diseased heart remains large in all stages, since it is not properly contracting.

The first column shows mid diastole, the second shows late diastole, and the third shows systole.

In mid diastole, the fluid entering through the mitral valve reaches the lower regions and causes the blood to circulate (figure 7 (a)). During late diastole, we see that a large amount of blood enters the healthy heart at high velocity (figure 7 (b)), causing significant turbulence and further circulation. Finally, as the heart fully constricts during systole, the fluid velocities everywhere remain high and the blood is adequately ejected (figure 7 (c)).

However, we see that in the case of the diseased heart, the inflow during diastole is significantly reduced and the blood in the apex is fairly stagnant (figure 7 (d), (e)). Then, in systole, we see again that the flow velocities are lower than that of the healthy heart and does not fully expel the blood (figure 7 (f)). This result would be extremely useful to a doctor, as this lack of circulation across all stages of the heart cycle presents a clear risk of clotting to the patient. We also note that the size of the diseased heart is larger than that of the normal heart, since the apex is not properly contracting during systole.

For a quantitative comparison, we seek the velocities around the trabeculae at the apex of the heart. To do this, we selected a small spherical region close to the trabeculae, and computed the velocity magnitudes within each cell in the sphere at each time step for both the healthy and diseased heart. We plot the results for two cardiac cycles in figure 8. Late diastole begins at approximately time steps 2 and 52, and systole begins at time steps 10 and 60. We see that, on average, the velocities in the diseased heart in this region are about half of those in the healthy heart. In particular, we see that during systole, the blood velocities at the apical region of the diseased heart tend not to increase as they do in the healthy heart, suggesting that this fluid is not being effectively expelled, creating a risk of clotting.

6. CONCLUSION

We have demonstrated how we can now model blood flow through hearts extracted from high-resolution CT data that contain very complex moving boundaries. We have also described a number of ways to visualize the modeled flow of blood through the heart, which can be extended and be useful to doctors in diagnoses and treatment plans. Finally, we have shown how these visualizations can be used to compare the simulated blood flow through a normal heart and one suffering from disease to show that how the abnormal heart may be at increased thrombosis risk due to noncirculating blood. In the future, we plan to perform similar visualizations on other models of diseased hearts derived from patient-specific CT data. In particular, we are looking to understand the movement of blood through trabeculae and detect risk of clots in

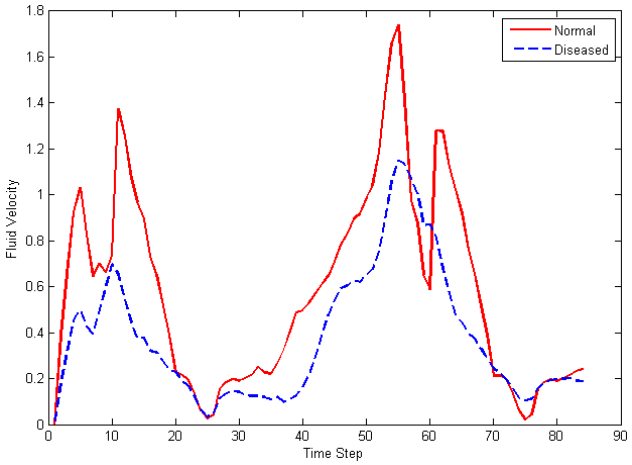

Fig. 8. Average magnitudes of velocities in the apex of the healthy and diseased heart during two cardiac cycles. Late diastole begins at approximately time steps 2 and 52, and systole begins at time steps 10 and 60.

these regions, and how clots may affect the flow.

7. ACKNOWLEDGMENTS

This material is based upon work supported by the U.S. Department of Homeland Security under Grant Award Number 2007-ST-104-000006. The views and conclusions contained in this document are those of the authors and should not be interpreted as necessarily representing the official policies, either expressed or implied, of the U.S. Department of Homeland Security.

8. REFERENCES

[1] Viorel Mihalef, Dimitris Metaxas, Mark Sussman, Vassilios Hurmusiadis, and Leon Axel, "Atrioventricular blood flow simulation based on patient-specific data," in *FIMH '09: Proceedings of the 5th International Conference on Functional Imaging and Modeling of the Heart*, Berlin, Heidelberg, 2009, pp. 386–395, Springer-Verlag.

[2] Viorel Mihalef, Razvan Ionasec, Yang Wang, Yefeng Zheng, Bogdan Georgescu, and Dorin Comaniciu, "Patient-specific modeling of left heart anatomy, dynamics and hemodynamics from high resolution 4d ct," in *ISBI'10: Proceedings of the 2010 IEEE international conference on Biomedical imaging*, Piscataway, NJ, USA, 2010, pp. 504–507, IEEE Press.

[3] "The visible human project," http://www.nlm.nih.gov.

[4] Timothy Jones and Dimitris Metaxas, "Patient-specific analysis of left ventricular blood flow," vol. 1496, pp. 156–166, 1998, 10.1007/BFb0056198.

[5] R. Merrifield Q. Long, P. J. Kilner G. Z. Yang, and X. Y.Xut D. N. Firmin, "The influence of inflow boundary conditions on intra left ventricle flow predictions," pp. 125, 922927, 2003.

[6] Gosman A. D. Merrifield R. Yang G. Z. Charrier C. Gatehouse P. Firmin D. Saber N., Wood N., "Progress towards patient-specific computational flow modeling of the left heart via combination of magnetic resonance imaging with computational fluid dynamics," pp. 31(1), 42–52, 2003.

[7] Nick Foster and Dimitri Metaxas, "Realistic animation of liquids," *Graph. Models Image Process.*, vol. 58, pp. 471–483, September 1996.

[8] Kensuke Yokoi, Feng Xiao, Hao Liu, and Kazuaki Fukasaku, "Three-dimensional numerical simulation of flows with complex geometries in a regular cartesian grid and its application to blood flow in cerebral artery with multiple aneurysms," *Journal of Computational Physics*, vol. 202, no. 1, pp. 1 – 19, 2005.

[9] Viorel Mihalef, Samet Kadioglu, Mark Sussman, Dimitris Metaxas, and Vassilios Hurmusiadis, "Interaction of two-phase flow with animated models," *Graph. Models*, vol. 70, no. 3, pp. 33–42, 2008.

[10] Mark Sussman, "A parallelized, adaptive algorithm for multiphase flows in general geometries," *Comput. Struct.*, vol. 83, no. 6-7, pp. 435–444, 2005.

[11] Diane de Zlicourt, Liang Ge, Chang Wang, Fotis Sotiropoulos, Anvar Gilmanov, and Ajit Yoganathan, "Flow simulations in arbitrarily complex cardiovascular anatomies - an unstructured cartesian grid approach," *Computers & Fluids*, vol. 38, no. 9, pp. 1749 – 1762, 2009.

[12] Anvar Gilmanov and Fotis Sotiropoulos, "A hybrid cartesian/immersed boundary method for simulating flows with 3d, geometrically complex, moving bodies," *J. Comput. Phys.*, vol. 207, no. 2, pp. 457–492, 2005.

[13] Viorel Mihalef, Dimitris Metaxas, and Mark Sussman, "Textured liquids based on the marker level set.," *Comput. Graph. Forum*, vol. 26, no. 3, pp. 457–466, 2007.

[14] Douglas Enright, Stephen Marschner, and Ronald Fedkiw, "Animation and rendering of complex water surfaces," *ACM Trans. Graph.*, vol. 21, no. 3, pp. 736–744, 2002.